VDMA
Fluid Power Association

22nd ISC

International Sealing Conference

Stuttgart, Germany
October 01 - 02, 2024

Sealing Technology –
Challenges accepted!

UNI STUTTGART

© 2024 VDMA Fluidtechnik
All rights reserved. No part of this publication may be reproduced, stored in retrieval systems or transmitted in any form by any means without the prior permission of the publisher.

ISBN 978-3-8163-0768-6

Fachverband Fluidtechnik im VDMA e. V. Lyoner Str. 18
50628 Frankfurt am Main
Germany

Phone +49 69 6603-1513
E-Mail maximilian.baxmann@vdma.org
Internet www.vdma.org/fluid

Additive Manufacturing of Sealing rings: Material Selection and Application Development

Jacqueline Gerhard, Lothar Hörl, Frank Bauer

The use of additive manufacturing, particularly 3D printing, for the production of seal rings is a promising way to speed up the development cycle of new products. In addition, this technology enables the rapid optimization and investigation of seal profiles. In order to guarantee the required sealing function, the sealing material must meet specific requirements. In this study, a comprehensive analysis is performed focusing on the evaluation of elastic 3D printable materials to gain an understanding of the general properties and behaviour of these materials. A liquid crystal display printer was used for all tests. The first prototypes of additive manufactured rod seals for a pneumatic application were tested.

1 Introduction

The use of additive manufacturing in the sealing technology allows for the rapid exploration and implementation of geometric variations in sealing profiles, enabling rapid optimization for individual applications. However, this manufacturing process presents new challenges. In order to guarantee the required sealing function, the sealing material must meet specific requirements and therefore it is important to fully understand the material behaviour.

In the following, the most common 3D printing techniques and the objective of this work will be explained. Chapter 2 will present the most significant results of the material tests, followed by the results of pneumatic rod seals on the test rig in chapter 3.

1.1 3D Printing Technologies

In the **Fused Deposition Modeling** (FDM) process, the material, a solid thermoplastic in the form of filaments, is melted in the extruder and applied through a nozzle onto the printing platform. After printing, the thermoplastic cools and hardens again.

In addition to the FDM process, there are processes in which liquid photosensitive resins are cured using some form of light energy, in the following called “resin printer”. These processes use a resin tank with a transparent film on the bottom and a non-stick surface. The resin tank contains the liquid resin. During the printing process, the printing platform is lowered into the resin tank. Some space is left between the bottom of the printing platform and the non-adhesive surface of the tank bottom. This space corresponds to the layer height. The liquid resin in the gap between the printing platform and the tank bottom is selectively exposed to light through the transparent film to cure the desired areas, leaving the remaining areas liquid. By moving the platform up, the hardened layer is separated from the tank bottom and new resin flows into the gap between the printing platform and the tank bottom. This process is repeated until printing is complete. The most common techniques that utilize UV light to cure photosensitive polymers are presented below.

In the **Stereolithography** (SLA) technique, a laser is used to selectively cure the resin by punctually laser scanning the surface. The **Masked Stereolithography** (mSLA) technique uses LEDs which are projected through a masking screen. The mask prevents light from passing through to create the curing pattern. Because the LCD (Liquid Crystal Display), i.e. the mask, absorbs most of the energy of the LEDs, the mSLA technology has a lower amount of energy per unit area but is generally a faster printing technique than SLA because the projector can expose the entire layer at once rather than curing point by point. **Digital Light Processing** (DLP) is a technique that uses a digital light projector as a light source to cure the resin. The projector shines its light onto the DMD (Digital Micromirror Device), which consists of thousands of small mirrors, each of which is capable of deflecting the light from the projector in a different direction. For each layer, these mirrors are arranged in a specific orientation that reflects the digital light beam from the projector onto the bottom of the tank in the shape of the layer to be printed.

Photopolymers for resin printers are UV-activated synthetic resins. During photopolymerization, the resin consisting of monomers and photo initiators is exposed to UV rays. The initiators are split into free radicals by the exposure. The free radicals cause the monomers to crosslink to form polymer chains. Components produced by photopolymerization exhibit anisotropic behavior, primarily due to inadequate crosslinking during layer formation.

Another process is **Selective Laser Sintering** (SLS), in which small polymer powder particles are sintered into a solid structure. For this process, powder is applied to the printing platform in a thin layer. The printer heats the powder to a temperature slightly below the melting point. The laser then scans the areas, which should be printed, and heats the powder which mechanically fuses the particles and creates a solid part.

In all additive manufacturing processes, layers are added sequentially, resulting in stepped structures on rounded or angled edges of the component. These are generally more pronounced when using FDM printers than when using resin printers. As example, an O-ring with a round cross-sectional geometry was printed with the mSLA printer Mono M5s from Anycubic and then measured with the IMA seal scanner [1]. For comparison, the same O-ring was printed using the FDM printer Sovol S06 with a layer height of 0.1 mm. The contour of the printed O-ring using FDM is shown in Figure 1 (left) and the contour of the printed O-ring using mSLA in Figure 1 (middle). For comparison, an injection-molded O-ring was measured, Figure 1 (right). The contours of the FDM printed O-ring are significantly more stepped than those of the mSLA printed O-ring. An injection-molded O-ring with smooth contours is more similar to an mSLA printed O-ring and the mSLA technique is therefore more suitable for printing seal rings.

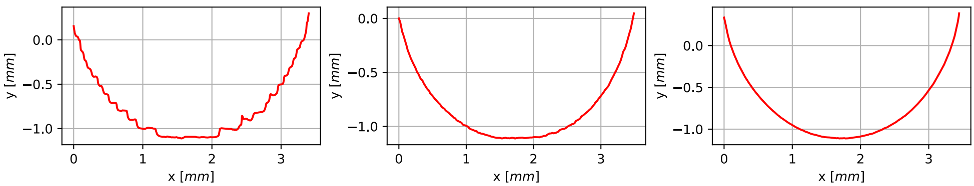

Figure 1: Geometry of printed O-rings: FDM (left), mSLA (middle) and of an injection-molded O-ring (right)

1.2 Objective

There have already been a few attempts to realize the additive manufacture of seal rings [2-7]. One approach is to print injection moulds and use them to produce seals in an injection moulding machine. There are various materials that are advertised for this purpose, for example the ultracure 3D RG 3280 from BASF or the Somos PerFORM material from Stratasys. However, this requires an injection moulding machine to be available. In addition, there exist different modifications of the standard printing processes presented in chapter 1.1. As example, Cubicure developed the Hot Lithography technique which can be used to print temperature-resistant and long-term stable moulds for an injection moulding machine. ViscoTec focuses on cross-linked chemistry and developed an extruder to print cross-linked 2-component materials. The acquisition costs for these systems are higher than those for standard resin printers, but they have already been used to successfully print seals [8].

In this study, the objective is to analyse the most straightforward approach and therefore the direct printing of seal rings. In order to achieve this, the first goal is to understand photopolymers for 3D printing and study how they behave under different conditions. Based on this, it will be possible to determine which type of seal they are suitable for. In the scope of this work, the focus was on one mSLA 3D printing technique and four pre-selected materials from two manufacturers. These materials will be used to investigate the behaviour and possibilities of the materials. A resin printer was chosen as this has significantly better printing accuracy than FDM printers.

2 Material property studies

Two Anycubic models were used as mSLA printers (Mono M5s and M3 Max). Tensile and compression set tests were performed on samples from both printers and no difference was found between the two mSLA printers when using the same resin. The printing parameters were initially set to achieve the most accurate printing of a test geometry. For example, the exposure time, the length of time each layer is exposed, depends on the material and must be adjusted for each material. If the exposure time is too short, either the desired area will not be fully cured, resulting in geometric deviations, or the layers will not adhere to each other and the part will fall off during the printing process. If the exposure time is too long, light scattering will cause areas outside the exposed area to cure. As a result, the parts are usually larger than defined in the Computer Aided Design (CAD) software.

The materials analysed are listed in Table 1. The Shore A hardness of the materials was measured according to DIN ISO 48-4 [10] on the day of printing (t_{storage} = 0 h) and 4 weeks later (t_{storage} = 4 w). These measurements are compared with the hardness specified in the manufacturer's data sheet. In the following, only the abbreviation in the second column is mentioned instead of the entire name of the materials.

Table 1: Materials and their Shore A hardness

		Shore A hardness		
Material	Abbreviation	t_{storage} = 0 h	t_{storage} = 4 w	Data sheet
Loctite 3D 8195	L 8195	59	60	58
Loctite 3D IND475	IND475	60	70	60
Resione F69	F69	73	95	60-75
Resione F80	F80	56	78	50-60

Based on the measured hardness listed in Table 1, changes in the materials over time were determined. Throughout the storage period, the specimens were stored at room temperature and protected from light. Ideally, the sealing material and therefore the sealing function of a seal should not change significantly over time. Therefore, a change of more than 20 Shore A in a 4-week period could render a material unsuitable as sealing material. After a further 4-weeks (t_{storage}= 8 w), this change in hardness was no longer detectable, indicating that the material could still be used as sealing material. Tensile tests were carried out for further analysis and the results are presented below.

2.1 Tensile Tests

As the materials cure under UV light, the material properties can still change after printing if the printed parts are exposed to sunlight. To analyse these material changes due to post-curing, tensile tests according to DIN 53504 [9] were performed. Figure 2 shows the geometry of the S2 test specimen with a thickness of 2 mm. Firstly, it was investigated how the stress-strain curve changes after the samples have been stored for a certain time at room temperature and protected from light. These changes were then tried to be reproduced by a longer exposure time or curing time. The samples were tested at a speed of 100 mm/min. Each variant was measured five times and then a representative curve, the most central, was selected from the five resulting measurements for further analysis. The technical strain and the technical stress are shown in the following.

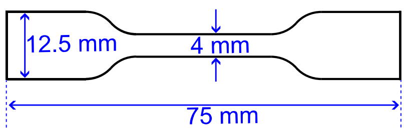

Figure 2: S2 Test specimen

To analyse the material changes due to post-curing, specimens made of IND475 were tested after different time intervals. The specimens were all printed at the same time and then stored for the time t_{storage} until they were tested. Figure 3 shows the measured stress-strain curves for different storage times t_{storage} between printing and testing. The stress-strain curve shifts upwards and the material becomes stiffer due to post-curing.

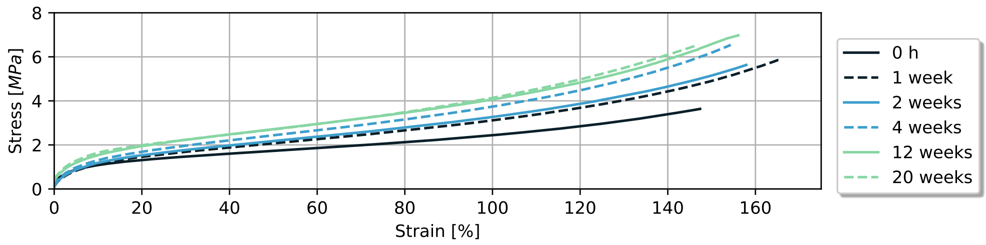

Figure 3: Tensile tests, IND475 Material, varying $t_{storage}$

In a further test, the curing time t_{cure} was increased to achieve a more cured state. The curing time defines how long the specimen is exposed to UV light in the curing station after printing in order to fully cure. The samples were all printed at the same time and then placed in the curing station for different lengths of time. In the curing station, the specimens are placed on a rotating plate and are exposed to UV light at a uniform wavelength of 405 nm from two angles. Afterwards they were immediately tested, the resulting stress-strain curves are presented in Figure 4. The upwards shift of the curve can also be observed with increasing t_{cure}, but is less significant than with increasing t_{storage}. After a longer curing time than 120 min, the samples became too brittle and broke between 80 % and 100 % strain. Therefore, longer times in the curing station were not further analyzed.

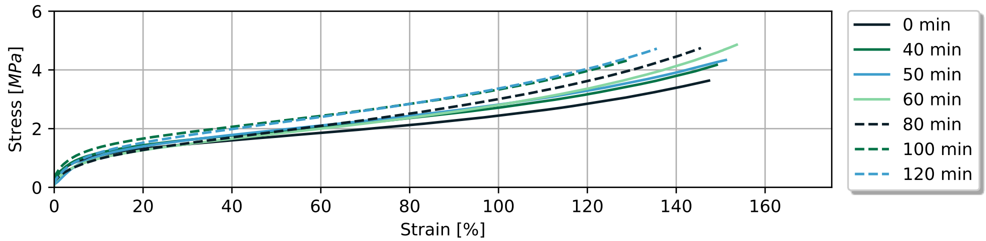

Figure 4: Tensile tests, IND475 Material, varying t_{cure}

As a third approach, the exposure time t_{exposure} with which each layer is exposed during printing was increased. Increasing the exposure time means that the geometry can no longer be reproduced well. Therefore, a sheet was printed and the samples were cut out of the printed sheet material. When increasing the exposure time, the effect of the upward shifted curve could not be observed for the material IND475. The differences in the stress-strain curves were too small to be recognized in the general scattering. The material behavior of F69 changes much faster with the storage time t_{storage} between printing and measurement, Figure 5. The upwards shift of the stress-strain curve is in the case of the F69 material also visible by increasing the exposure time t_{exposure}, Figure 6.

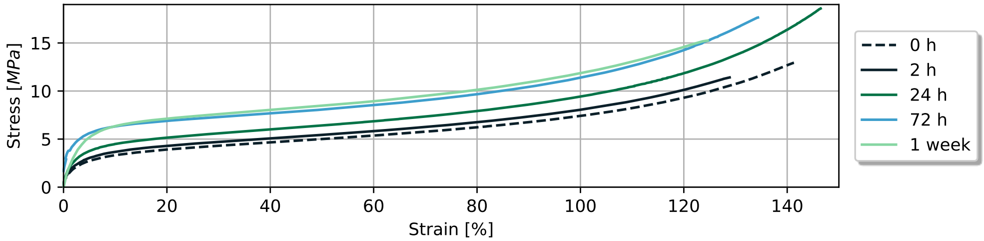

Figure 5: Tensile tests, F69 Material, varying $t_{storage}$

An increase in tensile strength of approximately 35 % was detected after only one week of storage for the F69 material, for which the greatest change over time was observed. For the IND475, the increase in tensile strength of approximately 20 % was measured after one week storage time and about 60 % after 20 weeks. For all tested materials from the resin printer, the change in material behaviour due to the storage time between printing and measurement was noticeable, but to different extents. For example, the upward shift in the stress-strain curve for the IND475 only became apparent after several days or weeks. In the case of the F69, the upward shift of the stress-strain curve was already visible after hours. This upward shift of the curve could also be caused by increasing the curing time. For some of the materials, the upwards shift could be reproduced by increasing the exposure time, but by a much smaller amount than by increasing the curing time. It was therefore not possible to prove that the change in material behaviour over time is only due to post-curing by UV light. Before testing, the tensile samples were weighed. A reduction in weight over time was observed for all materials. This indicates that the change over time is not only due to post-curing by UV light, but due to another effect.

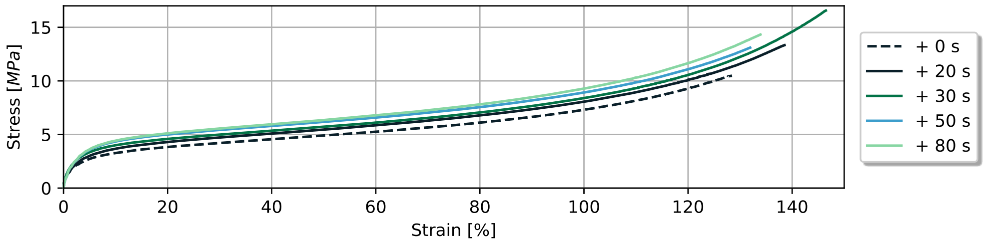

Figure 6: Tensile tests, F69 Material, varying $t_{exposure}$

An upward shift of the stress-strain curve of elastomers, and thus a higher stiffness, can be achieved by a higher loading speed [11]. A downwards shift can be achieved by higher temperatures [11]. At faster loading speeds, the stress-strain curve of the photopolymers is shifted upwards, meaning the behavior of the photopolymers is thus similar to that of elastomers. However, no reduced material stiffness was observed at higher temperatures.

2.2 Compression Set

The compression set (CS) was measured according to DIN 815 [12] at room temperature (RT), 55 °C and 85 °C. Cylindrical specimens with a diameter of 13 mm and a height of 6.3 mm were compressed by 25% for a period of 24 hours or 72 hours. For each variant five specimens were tested, the results shown hereafter are the average of the five measurements. For each material, the curing time t_{cure} was varied to reproduce different curing states. However, no correlation was found between the compression set and the curing times of t_{cure} = {10, 20, 30, 40} minutes. The first significant changes in the CS could only be determined for curing times of 60 minutes or more. In the following only the results of the materials IND475 and F69 are shown, as the CS for the two materials F80 and L 8195 ranged between 0 % and 2 % for all measurements and is therefore insignificantly small. For the F69 material, the CS ranged between 25 % and 30 % for the 24 h and 72 h tests at room temperature. For all tests at higher temperatures, the CS was less than 2 %.

For elastomers, the CS increases at higher temperatures [13]. This was not the case with the printed materials. Figure 7 shows the measured CS for samples cured after printing for curing times t_{cure} = {10, 60, 120} minutes. In each case, one day was waited between printing and measurement (t_{storage} = 1 day). The results of the measurements after t_{storage} = 20 weeks are also shown, in this case the curing time was set to t_{cure} = 10 minutes.

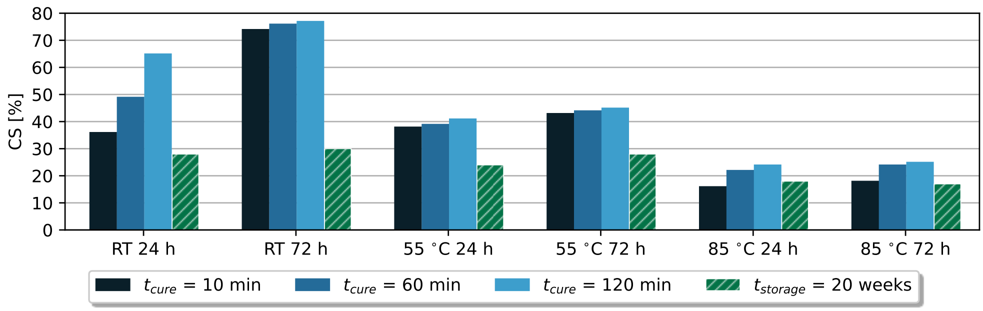

Figure 7: Compression set, IND 475

The CS increases for longer post-curing times t_{cure}. However, it decreases as the storage time t_{storage} between printing and testing increases. These results therefore indicate that the change in material behaviour over time is not just due to post-curing with UV light.

It could be that the materials are not yet fully cross-linked after printing. Testing at higher temperatures could accelerate the cross-linking, which is why the CS is lower at higher temperatures. At room temperature, the material does not fully cross-link during the test. Furthermore, the material behavior is different when it is cross-linked in a compressed state than when it is cross-linked in a relaxed state, which would explain the difference between the CS after longer curing times and after the storage time of 20 weeks.

The compression set at higher temperatures is generally lower for the IND475 material than at room temperature. Figure 8 shows the results for the F69 material at room temperature. At 55°C and 85°C, the CS ranged between 0 % and 2 %. As with the IND475 material, the CS of the F69 material decreases as the storage time t_{storage} increases. However, as the curing time t_{cure} increases, the CS increases.

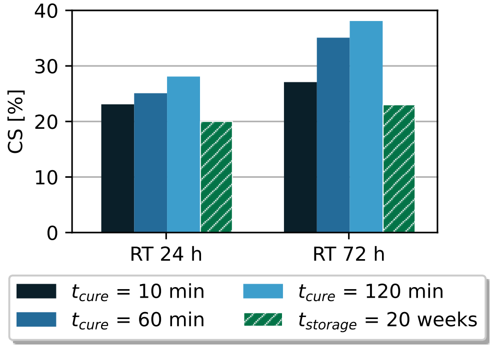

Figure 8: Compression set, F69

After the storage time of 20 weeks, the CS of the IND material decreases by 25 % in the 24-hour tests and by 60 % in the 72-hour tests at room temperature. In the case of the F69 material, the CS decreases about 15 % in both the 24-hour tests and the 72-hour tests at room temperature. In the tensile tests, the change in material behaviour over time was much more apparent for the F69 material than for the IND475 material. In the case of compression set the change over time is greater for the F69 material.

As defined in DIN 815, the CS was measured after 30 minutes. Figure 9 shows the results of the measurement in 5-minute steps from the time the samples were taken out of the steel plates for the 72-hour test at room temperature. The results of two polyurethane compounds from Parker Hannifin GmbH are shown for comparison.

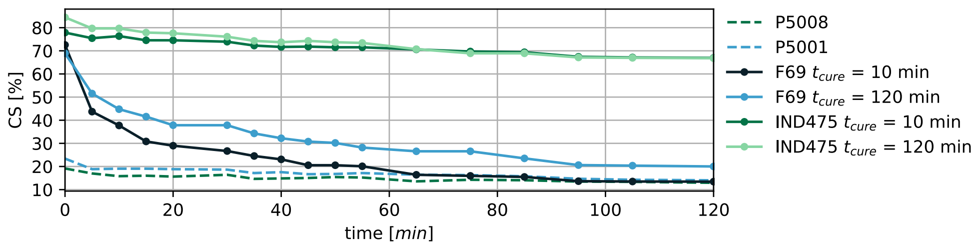

Figure 9: Compression set (72 h, room temperature) over time

The two polyurethane P5008 and P5001 from Parker Hannifin GmbH behave almost ideally. The CS is generally low and does not change much over time. The F69 material changes about 40 % in the first 40 minutes after removing the samples. The CS of the IND475 material decreases almost linearly and therefore similar to the Parker polyurethane. The samples made of IND475 and the samples made of polyurethane have probably deformed significantly within the first few seconds. This decrease within a few seconds was not measured. Thus, the material F69 takes longer to deform back, as the strong decrease of the CS occurs only after minutes. This indicates that the F69 specimens have not yet fully recovered after the 30-minute waiting time specified in DIN 815, which is a disadvantageous characteristic for a sealing material.

3 Additive Manufactured Rod Seals

A pneumatic rod seal design was printed from the four materials and analyzed. The test rig and the results of the reference seal are introduced below. This is followed by an explanation of the challenges encountered when printing the seal and the geometric optimization of the CAD file. The geometric optimization is then validated using the Finite Element Method (FEM).

3.1 Translational Test Rig

The frictional force between a seal ring and rod was measured at ambient pressure during horizontal movement of the rod on the translational test rig at the IMA. For this purpose, the ARUP seal ring [14] from Trelleborg Sealing Solutions for a rod diameter of 20 mm was printed. To obtain the CAD geometry the ARUP seal ring was cast in epoxy resin and the geometry measured. For all of the printed seal rings the same geometry file was used first, but had to be adapted later.

3.1.1 Reference Seal

The original ARUP seal ring from Trelleborg Sealing Solutions (TSS) made from a Polyurethan with 90 Shore A (WU9E1) was tested as reference. The seal rings were installed in a seal ring carrier first and then mounted on the rod. Next to the seal ring 0.1 ml of grease (Klübertemp GR M07 N) was then applied around the circumference of the rod. In a grease distribution run, the seal spreads the grease over the entire rod, after which the measurement was started. The frictional forces measured while moving the seal ring on the rod are shown in Figure 10 (left). For each variant, five seal rings have been tested. The frictional forces from the different seal rings are shown in different colors. During each measurement, the seal ring is moved 10 times with $v_{\max}$ = 200 mm/s from position x_{start}= 5 mm to position x_{end}= 70 mm which is why there are 10 curves for each tested seal ring. As the scatter between the five seal rings tested is very small and they all behave very similarly, the curves overlap. Figure 10 (right) shows the average frictional force and the scatter of the five seal rings. This was done by averaging the amount of the measurements taken at x = 35 mm. The minimum and maximum values of the measured force are marked by the grey bar. To analyze the force required at the beginning of the measurement and during the change of direction, the average of the amount of frictional force measured between x = 5 mm and x = 7 mm was calculated. The maximum value of the measured force in the range x = [5,7] mm is marked by the grey bar.

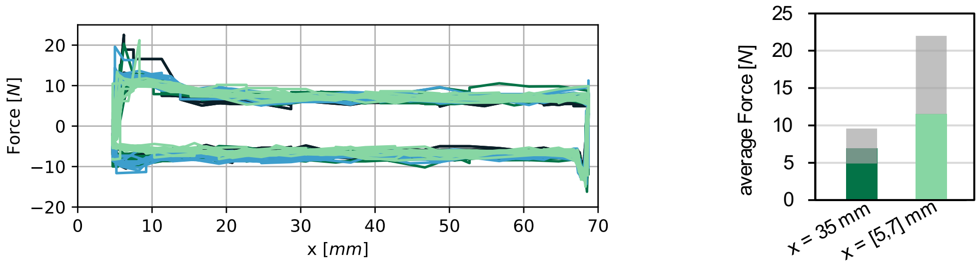

Figure 10: Measured frictional force (left) and average frictional force (right), seal rings from Trelleborg Sealing Solutions

3.1.2 Geometric Optimizations

When using an mSLA printer without optimizing the CAD geometry, printed parts tend to be oversized. In general, the first layers are exposed longer to ensure the components adhere to the printing plate. As a result, the first layers are printed larger, which can be corrected by a respective change in the CAD file. In addition to the oversize of these first layers, it was noted that the inner diameters of the printed seals were too small and the outer diameters too large. Therefore, these had to be adjusted as well. The printed seal rings were measured to determine the true inner diameter and the inner diameter in the CAD file was then adjusted. Figure 11 shows the sectional geometry of the seal ring. As an example, three dimensions are illustrated, which were adjusted in the CAD file in order to print the original geometry as accurately as possible. Using the diameters $d1_{\mathrm{CAD}}$ and $d2_{\mathrm{CAD}}$ listed in Table 2, an inner diameter of $d1_{\mathrm{printed}}$ = 19.5 mm ± 0.05 mm and an outer diameter of $d2_{\mathrm{printed}}$ = 29.5 mm ± 0.1 mm could be achieved for the printed seals. The width b of 3.6 mm could be achieved for all printed seals.

Table 2: Dimensions defined in the CAD file and actual measured dimensions [mm]

	$d1_{\mathrm{CAD}}$	$d1_{\mathrm{printed}}$	$d2_{\mathrm{CAD}}$	$d2_{\mathrm{printed}}$	b_{CAD}	b_{printed}
IND475	20.4	19.45	28.9	29.6	3.2	3.6
L 8195	19.3	19.5	29.4	29.5	3.6	3.6
F69	19.4	19.45	29.4	29.5	3.45	3.6
F80	19.6	19.5	29.3	29.5	3.5	3.6

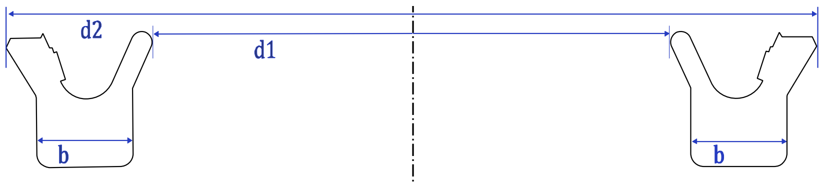

Figure 11: Sectional view of the seal ring

Despite the adjustment of the geometry according to Table 2, the shape of the sealing lip still deviates from the actual shape in the CAD file. Thus, the geometry of the seal ring made of IND475 was further optimized, as this was the geometry that deviated the most from the original geometry. Figure 12 (left) shows the measured frictional forces for the first printed seals with an inner diameter of $d1_{\mathrm{CAD}}$ = 19.5 mm in the CAD file and an average inner diameter of $d1_{\mathrm{printed}}$ = 18.5 mm measured on the printed seals. After adapting the geometry in the CAD file according to Table 2, an average inner diameter of $d1_{\mathrm{printed}}$ = 19.45 mm was measured, which significantly reduced the frictional force, Figure 12 (middle). Casting the printed seal rings in epoxy resin and measuring the printed geometry showed that the printed sealing lip was still too wide. The design of the sealing lip was then adjusted in the CAD file, which led to the frictional forces shown in Figure 12 (right).

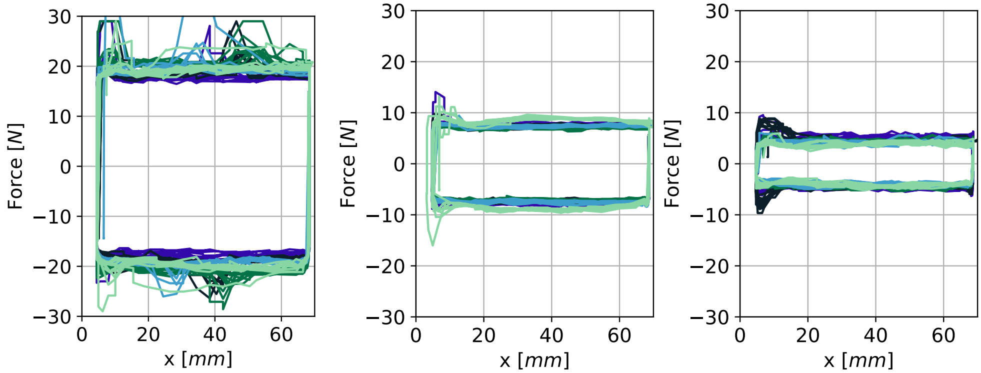

Figure 12: Frictional force, IND475, first printed seal (left), optimization of the diameters (middle) and adjustment of the sealing lip (right)

Thus, depending on the material, the geometry defined in the CAD file must first be adapted before a seal ring can be printed accurately using an mSLA printer.

Figure 12 also shows how quickly a seal geometry can be modified to achieve specific characteristics, such as lower friction. With a 3D printer, these geometry changes can be made fast and without much effort.

3.1.3 Material Comparison

For the 3D-printed seal rings, the printing parameters were selected for which the best accuracy could be achieved in printing tests. In order to test all seals under the same conditions, exactly seven days were waited between printing and testing. Figure 13 compares the frictional forces of the seals made of L 8195, F69 and F80. The diameters of the seal geometries have been adjusted to match the inner diameter of the original ARUP seal.

The individual seal rings made from L 8195 behave very differently, but the measurement results of a single seal ring vary only slightly. In the case of F69, it is the opposite: The five seal rings made of F69 all behave in a similar way, but the dispersion of one seal ring is greater.

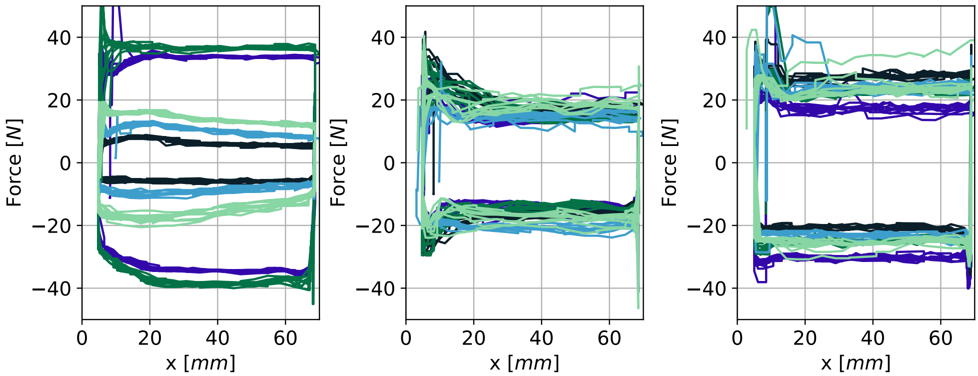

Figure 13: Frictional force, L 8195 (left), F69 (middle) and F80 (right)

In Figure 14, the average frictional force and the scatter is shown for the

- reference seal ring from Trelleborg (TSS),
- seal rings made of Loctite 8195, Resione F69 and Resione F80,
- Loctite IND475 seal rings, without geometric optimizations (IND475_1),
- Loctite IND475 seal rings with the optimization of the diameter (IND475_2),
- Loctite IND475 seal rings with the adjustment of the sealing lip (IND475_3).

The average of the five measurements at position x = 35 mm is displayed by the darker color. The average of the amount of frictional force measured between the positions x = 5 mm and x = 7 mm is displayed in a lighter color. The scattering, marked by the gray bar, is greatest for Loctite 8195. The Loctite IND 475 seals showed the lowest scatter, even without adjusting the geometry. In addition, the difference between the frictional force during movement (at position x = 35 mm) and the frictional force required to change direction (in the range x = [5,7] mm) is lowest for the seal rings made of Loctite IND 475.

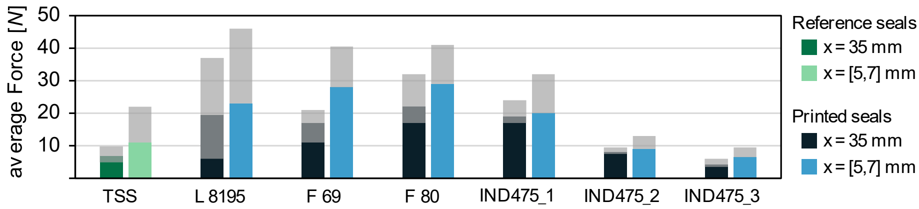

Figure 14: Average frictional force

In order to analyse the impact of the storage time on the frictional force, experiments were run with seal rings after t_{storage} = {0, 1, 4, 16} weeks. No trend in any direction could be recognized for the materials IND475, F69 and F80. The measured frictional forces of the seals made of L 8195 were generally so scattered that no trend could be identified either. The longest test run lasted 24 hours. The only seals that could not withstand this test run were made of the L 8195 material. These have torn after 18-21 hours. None of the other seals broke or showed signs of wear. In addition to the results shown in this chapter, measurements were performed under pressure. With the exception of the seals made of L 8195 material, all seals were able to withstand a pressure of 6 bar.

3.2 Assembly Simulation

The geometric optimizations of the seals made from IND475 were evaluated using the Finite Element Method (FEM). The actual printed geometries were measured and used. The measured frictional forces for these geometries are shown in Figure 12. The frictional force measured on the test rig can be calculated by

$$F_{\text{fric}} = \mu \; F_{\text{N}} \tag{1}$$

with the coefficient of friction μ and the contact normal force F_{N}. In an FEM simulation in the software MSC Marc Mentat, the assembly of the 2-dimensional cross-sectional geometry of the seal ring was simulated to get the contact normal force between seal ring and rod. To do so, the printed geometry was measured in order to ensure the same conditions as in the experiments. The seal ring carrier, in which the seals are installed before they are mounted on the rod, was also measured. In the FEM simulation, as in the experiments, the seal ring was first pushed into the groove, i.e. the seal ring carrier. The installed seal ring is then mounted on the shaft. The used Ogden material model is based on the tensile tests of the IND475 material at room temperature after t_{storage} = 1 week. Relaxation was not considered. The simulation results of the seal rings

- TSS: Reference seal ring, measurements shown in Figure 10
- IND475_1: First printed seal, measurements shown in Figure 12 (left)
- IND475_2: Optimization of the diameters, measurements Figure 12 (middle)
- IND475_3: Adjustment of the sealing lip, measurements Figure 12 (right)

are discussed in the following. Figure 15 shows the simulated installed seal ring IND475_3. The colors represent the first component of stress. Figure 16 shows the simulated contact forces between the sealing lip and shaft. The position x = 0 is defined by the node located left of the first node in contact with the shaft. The maximum values of the simulated normal force $F_{\mathrm{N,max}}$ are listed in Table 3. In addition, the frictional forces F_{fric} measured on the test rig are given. These are the average of all frictional forces measured between the two positions 20 mm and 40 mm.

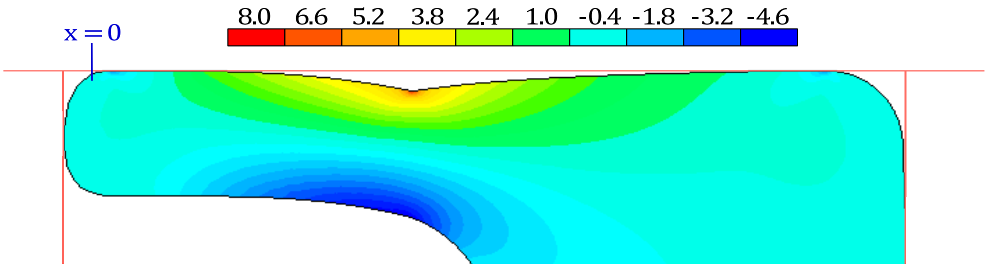

Figure 15: Simulation result, mounted seal IND475_3, 1st Component of Stress [N/mm^2]

The radial force, i.e. the force with which a seal ring is pressed against the shaft over the entire circumference, was measured using a radial force gauge [15] according to DIN 3761-9. Five seal rings were measured in each case, the average radial forces are given in in Table 3. When measuring the radial force, a higher value is measured at the beginning. Due to relaxation, the radial force decreases after only a few seconds. The values given in in Table 3 are the radial forces measured at the beginning, as no relaxation was considered in the simulation.

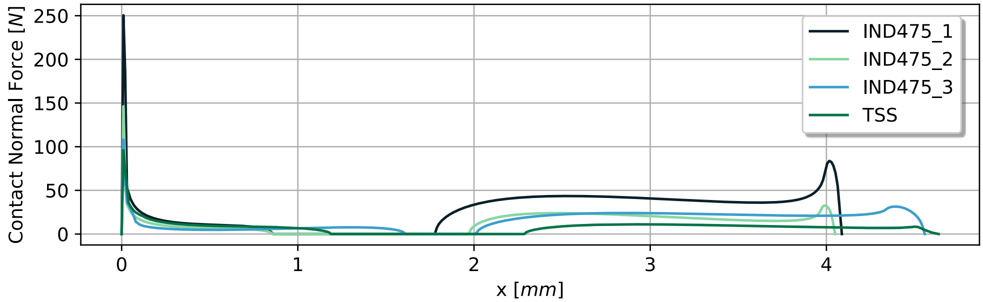

Figure 16: Simulation result, Contact Normal Forces of the sealing lip

Table 3: Frictional Forces measured on the test rig, Contact Normal Force obtained from the simulations and measured radial force

IND475_1	IND475_2	IND475_3	TSS
F_{fric} = 19 N	F_{fric} = 12 N	F_{fric} = 9 N	F_{fric} = 8 N
$F_{\mathrm{N,max}}$ = 251 N	$F_{\mathrm{N,max}}$ = 146 N	$F_{\mathrm{N,max}}$ = 108 N	$F_{\mathrm{N,max}}$ = 96 N
F_{radial} = 241 N	F_{radial} = 138 N	F_{radial} = 102 N	F_{radial} = 94 N

The measured radial forces agree well with the simulation results. Both the radial force and the frictional force could be significantly reduced by adjusting the inside diameter and optimizing the geometry of the sealing lip. Calculating the coefficient of friction from either the measured radial force F_{radial} or the simulated contact force $F_{\mathrm{N,max}}$ according to equation (1), results in a coefficient of friction between 0.076 and 0.088. These values are reasonable for a fully lubricated steel rod. On the test rig the same rod was used for all tests and the same amount of grease was applied. In the simulations, the same conditions were defined, the only change was the geometry of the seal. Therefore, the coefficient should be exactly the same. Small differences may be due to inaccurate measurement of the geometry.

4 Conclusion

The potential of additive manufacturing of seal rings using an mSLA printer was investigated. Additive manufacturing opens up many new possibilities in sealing technology. New and complex geometries can be produced and different geometric variations can be realized quickly. However, in order to fully exploit the potential, some preliminary work must be done first. This includes finding the right material, as there are many different photopolymers for mSLA printers available on the market.

The 3D-printed materials analyzed in this study have a lower elongation at break and a much lower tensile strength than conventional sealing materials. Nevertheless, the elongation at break of the printed materials is still sufficient for seals. In addition, very good Compression Set values were measured for the printed materials. One disadvantage is the change of the material behavior over time. All tested materials show a stiffer behavior in tensile tests after a longer period of time between printing and testing. The compression set is reduced by a longer waiting time, which is generally beneficial, but this still makes the material difficult to evaluate. The material change could not be reproduced by increasing the curing time or the exposure time, indicating that the change in material behavior was not due to post-curing with UV light. Before the materials can be used reliably, it is important to gain an understanding of the reason for their behavior. The change in material behavior could be due to reactions with the surrounding environment. Further tests need to be carried out, for example after storage times in a vacuum chamber, in order to detect evaporation of solvents out of the printed material.

The advantage, on the other hand, is the geometrical flexibility. For example, the sealing lip width can be changed very quickly to achieve the desired contact pressure between the sealing lip and the rod. In order to be able to do this, it is necessary to know how the geometry will be printed. Due to geometric deviations, the geometry file must be adapted depending on the printer and the material. If this is neglected, the geometry of the printed seal will not match the desired geometry which can lead to a poorer sealing performance. The impact of the geometric deviations on the frictional force between the seal and the rod was proven within the scope of this study.

It should be noted that the samples for all material tests were manufactured using an mSLA printer with a 405 nm light source. Printing on a different printer with a different light source may result in different material properties depending on the wavelength for which the material has been optimized by the manufacturer.

5 Acknowledgements

The authors thank the Fluid Power Research Fund of the VDMA for its financial support (grant: FKM No.7058300).

6 Nomenclature

Variable	***Description***	***Unit***
b_{CAD}	Width defined in the CAD file	[mm]
b_{printed}	Width measured on the printed seal	[mm]
$d1_{\mathrm{CAD}}$	Inner diameter defined in the CAD file	[mm]
$d1_{\mathrm{printed}}$	Inner diameter measured on the printed seal	[mm]
$d2_{\mathrm{CAD}}$	Outer diameter defined in the CAD file	[mm]
$d2_{\mathrm{printed}}$	Outer diameter measured on the printed seal	[mm]
F_{fric}	Frictional force	[N]
F_{N}	Contact normal force	[N]
t_{cure}	Curing time	[s]
t_{exposure}	Exposure time	[s]
t_{storage}	Storage time	[s]
v_{max}	Maximum velocity	[mm/s]
x_{start}	Start position of measurement	[mm]
x_{end}	End position of measurement	[mm]
μ	Coefficient of friction	[-]

7 References

[1] University of Stuttgart - Institute of Machine Components, “IMA-Sealscanner® (IMA-TechSheet #102050 V2)“. Accessed: 2. May 2024. [Online]. Available at: https://www.ima.uni-stuttgart.de/dokumente/forschung/dichtungstechnik/einrichtungen/en/102050en.pdf

[2] M. Graf, T. Ebel, T. Lankenau, K. Ottink, “Towards additively manufactured dynamic rod seals” in Proc. 21st Int. Sealing Conference 47-62, October 2022, doi: 10.61319/W7SZ07FJ

[3] T. Ebel, T. Lankenau, L.Sundermann, K. Ottink, et al. „Functional testing of entirely additively manufactured two-component hydraulic rod seals made of TPU and NBR” in *Discover Mechanical Engineering*, February 2024, doi: 10.1007/s44245-024-00034-x

[4] L. Sundermann, et al., “Tailoring the Curing Kinetics of NBR-Based Rubber Compounds for Additive Manufacturing of Rod Seals“, Advances in Polymer Technology, Bd. 2023, S. 1–16, August 2023, doi: 10.1155/2023/7343194

[5] A. Zhong, A. Phan, C. Glaesman, “World’s First 3D Printed Functional Polymeric Sealing Solutions“, in *Day 2 Tue, October 27, 2020*, October. 2020, doi: 10.2118/201573-MS

[6] D. Luning-Prak, B. Baker, und J. Cowart, “Engine O-Rings Produced Using Additive Manufacturing“, presented at the WCX SAE World Congress Experience, Detroit, Michigan, United States, April 2023, S. 2023-01–0893. doi: 10.4271/2023-01-0893

[7] B. Engendahl, C. Leibig, “3D Printing Flexible Materials: From Prototyping to Industrial Manufacturing”, Presentation at the 21st ISC 2022, Stuttgart

[8] ISGATECH GmbH, “Dichtungen drucken? Ja“, Dicht! Dichten.Kleben.Polymer.verstehen, Nr. 4.2023, ISSN: 1863-4699

[9] DIN German Institute for Standardization, “DIN ISO 48-4, Rubber, vulcanized or thermoplastic – Determination of hardness – Part 4: Indentation hardness by durometer method (Shore hardness)“. Beuth publishing DIN, February 2021

[10] DIN German Institute for Standardization, “DIN 53504:2009-10, Testing of rubber - determination of tensile strength at break, tensile stress at yield, elongation at break and stress values in a tensile test“. Beuth publishing DIN, October 2009

[11] F. Bauer, „Federvorgespannte-Elastomer-Radial-Wellendichtungen. Grundlagen der Tribologie & Dichtungstechnik, Funktion und Schadensanalyse“, Springer Vieweg, Wiesbaden, 2021, ISBN 978-3-658-32921-1, doi: 10.1007/978-3-658-32922-8

[12] DIN German Institute for Standardization und International Organization for Standardization, “DIN ISO 815-1:2022-04, Rubber, vulcanized or thermoplastic - Determination of compression set - Part 1: At ambient or elevated temperatures“. Beuth publishing DIN, April 2022

[13] U. Blobner, B. Richter, “Fachwissen Prüfverfahren für Elastomere – Druckverformungsrestprüfung“, O-Ring Prüflabor Richter GmbH, June 2015

[14] Trelleborg Group, “Trelleborg Sealing Solutions - Pneumatic Seals catalog“, 2011.

[15] University of Stuttgart - Institute of Machine Components, “Radialkraftmessgerät Desktopversion (IMA-TechSheet #102100 V2)“. Accessed: 8. May 2024. [Online]. Available at: https://www.ima.uni-stuttgart.de/dokumente/forschung/dichtungstechnik/einrichtungen/102090_102100.pdf

8 Authors

University of Stuttgart, Institute of Machine Components (IMA)

Pfaffenwaldring 9, 70569 Stuttgart, Germany:

Jacqueline Gerhard, M. Sc., ORCID 0000-0002-4879-5653,
Jacqueline.gerhard@ima.uni-stuttgart.de

Dipl.-Ing. Lothar Hörl, ORCID 0000-0002-2851-3364,
lothar.hoerl@ima.uni-stuttgart.de

apl. Prof. Dr.-Ing.Frank Bauer, ORCID 0000-0001-7799-7628,
frank.bauer@ima.uni-stuttgart.de

https://doi.org/10.61319/VC628LDF